We are IntechOpen, the world's leading publisher of Open Access books Built by scientists, for scientists

6,900
Open access books available

186,000
International authors and editors

200M
Downloads

Our authors are among the

154
Countries delivered to

TOP 1%
most cited scientists

12.2%
Contributors from top 500 universities

BOOK CITATION INDEX — CLARIVATE ANALYTICS — INDEXED

WEB OF SCIENCE™

Selection of our books indexed in the Book Citation Index
in Web of Science™ Core Collection (BKCI)

Interested in publishing with us?
Contact book.department@intechopen.com

Numbers displayed above are based on latest data collected.
For more information visit www.intechopen.com

Collapse Load for Thin-Walled Rectangular Tubes

Kenichi Masuda and Dai-Heng Chen

Additional information is available at the end of the chapter

Abstract

In this chapter, thin-walled rectangular tubes under pure bending are considered, by performing a series of FEM numerical studies. In the simulation, a homogeneous and isotropic elastic perfectly plastic material was employed for the tube material. A commonly used method for predicting the collapse load of rectangular tubes subjected to pure bending was proposed by Kecman. Kecman's method focuses on a slenderness of the flange. When buckling occurs in the flange, this method uses a collapse load corresponding to the post buckling strength of the flange. When buckling does not occur at the flange, this method used a relation of the flange slenderness to the cross-sectional fully plastic yielding. This method for predicting the collapse loads is effective when the aspect ratio of web to flange is not large. However, for large aspect ratios, there is a large discrepancy between the values of maximum moment corresponding to the collapse loads obtained from this method and the FEM numerical results due to an effect of web slenderness. A new method is proposed to predict the maximum moment considering the effect of web slenderness. The validity of the collapse load estimation is checked by the results of FEM numerical simulation.

Keywords: thin-walled tube, bending, buckling, collapse load, fem

1. Introduction

The aims of this chapter are as follows:

- To understand the validity of existing estimation methods [1] by using the results of numerical simulations.

- To point out a case in which the estimation method is not applicable by using the results of numerical simulations.

- To understand a factor of the discrepancy by using the results of numerical simulations.

- To propose a new estimation method by considering the factor and using mathematical approach.

- To understand the validity of the new estimation method by comparing with the results of numerical simulations.

We selected "Collapse load for thin-walled rectangular tubes under bending" as the subject of these topics. The research content of this chapter is based on our recent paper [2], and this chapter shows the results of numerical simulations in detail.

2. To understand the validity of existing estimation methods by using the results of numerical simulations

2.1. Numerical simulation method

Figure 1(a) shows the simulated rectangular tubes, in which one end of the rectangular tube was fixed to a rigid wall, and pure bending was applied from the other end by modeling a lid rotating about the z axis under rotary control θ. Bending moment M can be derived from the rigid wall as reaction moment. **Figure 1(b)** shows a deformation shape and bending angle θ. Until buckling occurs, axial strain ε_x can be defined by

$$\varepsilon_x = \frac{\theta}{L} y \tag{1}$$

Figure 1(c) shows the axial strain distribution ε_x on cross-section for a square tube with $t = 0.4$ mm, $a = b = 50$ mm at $\theta/L = 0.01$ m^{-1}. As shown in **Figure 1(c)**, the axial strain distribution ε_x of FEM is in good agreement with the value obtained from Eq. (1). The effects of various geometric parameters were investigated under bending collapse. These parameters were tube thickness t, width of the flange a, and width of the web b. In order to prevent torsional behavior, a rigid lid was adopted as suggested by Guarracino [3]. In particular, the lid thickness t_f was set to five times of t. In the simulation, a homogeneous and isotropic elastic perfectly plastic material was employed for the tube material. As a yield condition, von Mises yield conditions were adopted. In this chapter, the material mechanical properties are set as follows. Young's modulus E is set as 72.4 GPa, the yield stress σ_s is set as 72.4 MPa, and Poisson's ratio ν is set as 0.3.

In this chapter, in order to formulate the geometric nonlinear behavior and solve the nonlinear equation, the updated Lagrange method, algorithm based on the Newton–Raphson method, and return-mapping method were used. The rectangular tubes were meshed using four-node quadrilateral thickness shell elements (Element type 75) with five integration points across the thickness. A convergence test on element size was conducted, and the adopted divide method was that the wall width divided into at least 20 sublengths, and the wall length divided as the elements become almost square.

In order to neglect the influence of the boundary conditions, the ratio of the length and width L/a, L/b was set to $L/a > 6$, $L/b > 6$. It means that the length of tubes was assumed to be large enough.
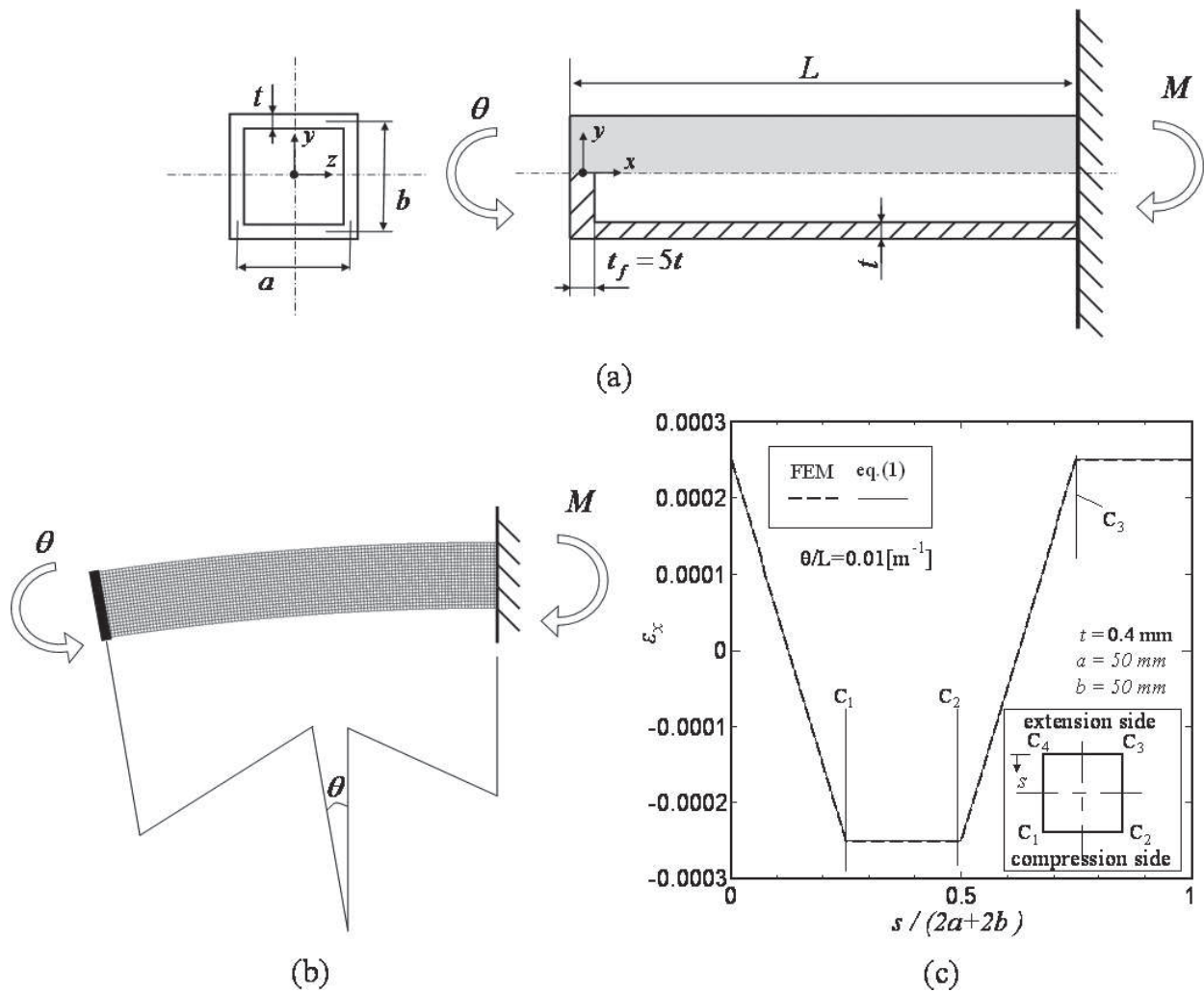
Figure 1. Numerical simulation model: (a) rectangular tube to which a pure bending moment is applied; (b) deformed shape; and (c) axial strain distribution on cross-section at $\theta/L = 0.01$ m^{-1}.

2.2. Kecman's method for predicting the maximum bending moment of rectangular tubes

Kecman focused on slenderness corresponding to buckling stress of the compression flange and proposed a formula to predict the collapse load or the maximum moment M_{max}. Depending on the value of buckling stress σ_{buc-a} of the compression flange

$$\sigma_{buc-a} = \frac{k_a \pi^2 E}{12(1 - v^2)} \left(\frac{t}{a}\right)^2 \qquad (2)$$

three cases are distinguished, as shown in **Figure 2**. In Eq. (2), k_a is the buckling coefficient, which Kecman assumed to be
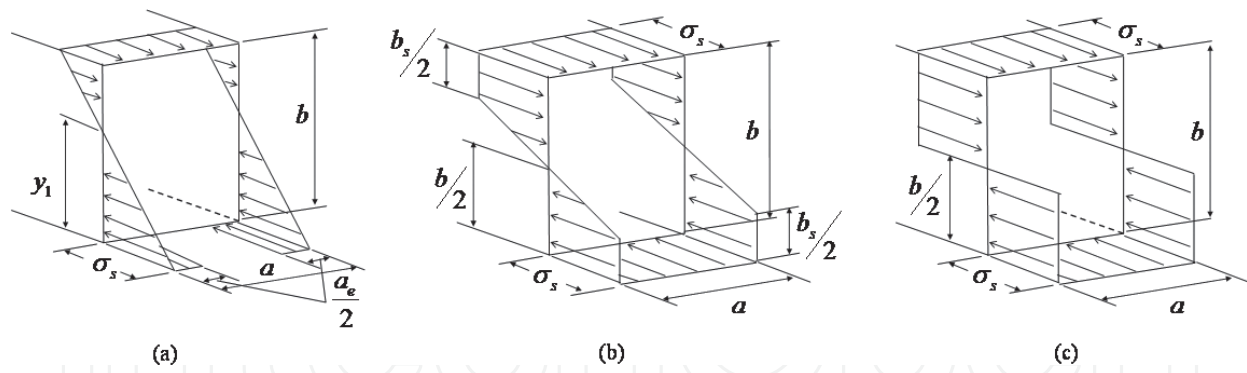
$$k_a = 5.23 + 0.16 \frac{a}{b} \qquad (3)$$

Figure 2. Schematic representation of axial stress distribution is used in the Kecman's method: (a) case 1: $\sigma_{buc\text{-}a} < \sigma_s$; (b) case 2: $\sigma_s < \sigma_{buc\text{-}a} < 2\sigma_s$; and (c) case 3: $\sigma_{buc\text{-}a} > 2\sigma_s$.

The maximum moment M_{max} for the rectangular tube is given by

$$M_{max} = \sigma_s tb^2 \frac{2a + b + a_e\left(3\frac{a}{b} + 2\right)}{3(a + b)} \tag{4}$$

For Case 1

$$M_{max} = M_{el} + \left(M_{pl} - M_{el}\right)\frac{\sigma_{buc\text{-}a} - \sigma_s}{\sigma_s} \tag{5}$$

For Case 2, and

$$M_{max} = M_{pl} \tag{6}$$

For Case 3. In the above equations

$$a_e = a\left(0.7\frac{\sigma_{buc\text{-}a}}{\sigma_s} + 0.3\right) \tag{7}$$

and M_{el} and M_{pl} are the maximum elastic moment

$$M_{el} = \sigma_s tb\left(a + \frac{b}{3}\right) \tag{8}$$

and the cross-sectional fully plastic bending moment

$$M_{pl} = \sigma_s tb\left(a + \frac{b}{2}\right) \tag{9}$$

respectively.

Figure 3 shows a flow chart of the Kecman's method for predicting the maximum moment of tubes under pure bending.

2.3. The applicability of the Kecman's method for square tubes

Figure 4 shows that the bending moment M and the axial stress σ_x on cross-section for a square tube with $t = 0.4$ mm, $a = b = 50$ mm are subjected to pure bending ($\sigma_{buc\text{-}a} = 0.31\sigma_s < \sigma_s$). In order to better understand the bending collapse, Eq. (4) for Case 1 and the elastic buckling stress
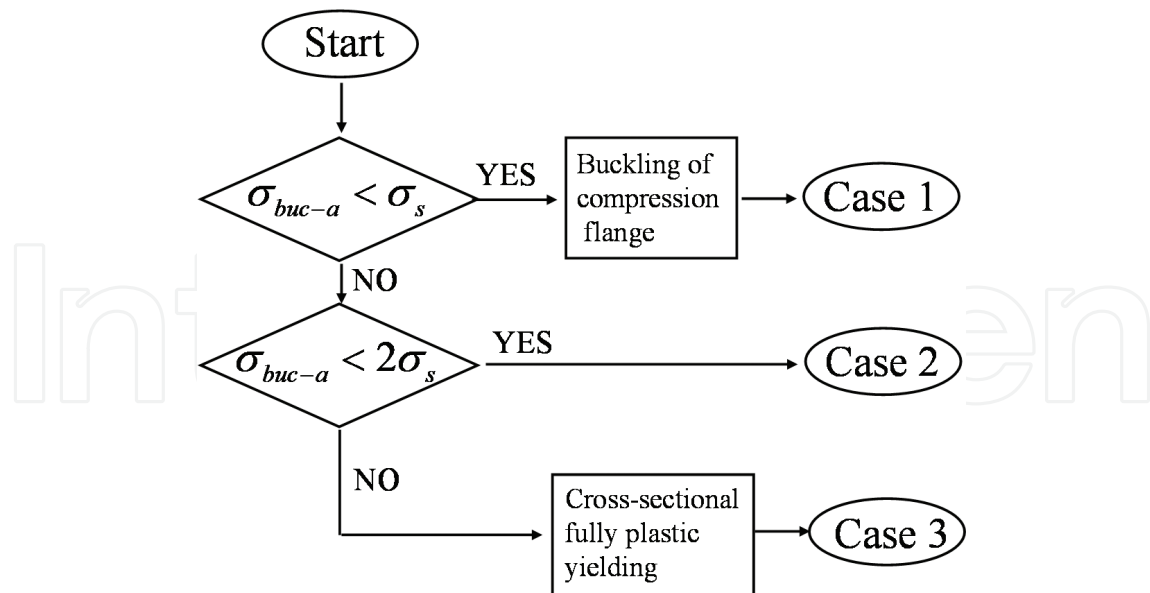
Figure 3. Flow chart of the Kecman's method for predicting the maximum moment of tubes under pure bending.

σ_{buc-a} given by Eq. (2) are also shown as a comparison. As shown in **Figure 4(a)**, the maximum moment of FEM is in agreement with Eq. (4). The maximum value of σ_x at point P is in good agreement with Eq. (2). In addition, the axial compression stress σ_x at point Q at the quarter-web width keeps increasing after buckling occurs at point P in the middle of the compression flange, and the maximum value of σ_x at point Q occurs in the maximum moment. Moreover, as shown in **Figure 4(b)**, although the axial compression stress in the middle of the compression flange decreases due to buckling at the flange, the axial compression stress increases at
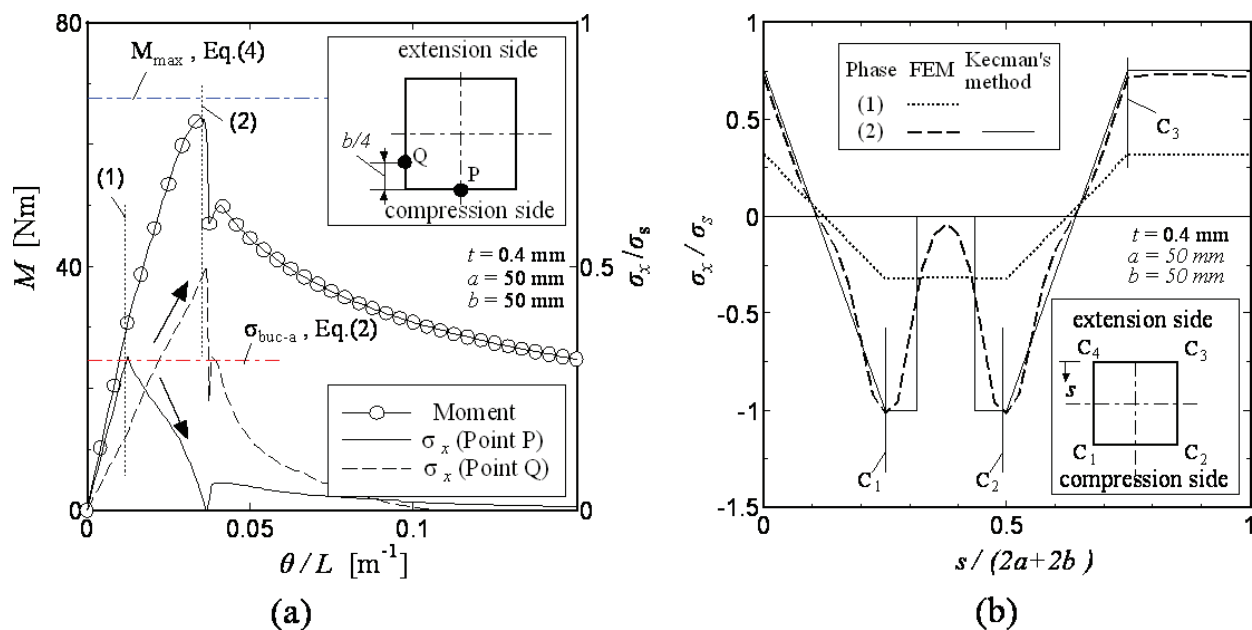

Figure 4. Moment M and axial stress σ_x on cross-section for a square tube with $t = 0.4$ mm, $a = b = 50$ mm are subjected to pure bending: (a) changes in moment M and axial stress σ_x at points P and Q on cross-section and (b) axial stress distribution on cross-section at phases (1) and (2) corresponding to $\theta/L = 0.012$ m^{-1} and $\theta/L = 0.038$ m^{-1}, respectively, as denoted in (a).

both edges of the flange due to a corner constraint at the edges. Just after buckling, the stress increment at both edges is greater than the stress decrement in the middle of the compression flange, and thus the total force on the compression side increases and the moment increasing continuously. It is also noted that the stress on the web changes almost linearly; this suggests that buckling does not occur at the web. Therefore, the axial stress distribution when the maximum moment occurs is in good agreement with that obtained by the Kecman's method using the effective width of the compression flange, as shown by the solid line in the figure.

The above investigation confirms that for such tubes with b/a = 1 and $\sigma_{buc-a} < \sigma_s$, collapse is due to buckling at the compression flange, and the maximum moment can be predicted by the Kecman's method for Case 1.

Figure 5 shows the bending moment M and the axial stress σ_x on cross-section for a square tube with $t = 0.9$ mm, $a = b = 50$ mm ($\sigma_{buc-a} = 1.52\sigma_s > \sigma_s$). As shown in **Figure 5(a)**, the maximum moment is in good agreement with the value obtained from Eq. (5) for Case 2. The maximum value of σ_x at point P and Q occurs in the maximum moment and σ_x/σ_s at point P becomes 1. Moreover, as shown in **Figure 5(b)**, the absolute value of the axial stress at phase (2), for which the maximum moment occurs, is greater than the value at phase (1) for all cross-sectional positions. At phase (2), the stress at the flanges is equal to the yield stress σ_s, and there also exist plastic yielding regions in the webs. In **Figure 5(b)**, Kecman's stress distribution when the maximum moment occurs is obtained by linear interpolation of two theoretical stress distributions corresponding to M_{el} and M_{pl}, respectively, and is shown by a solid line. It is seen from **Figure 5(b)** that the axial stress distribution when the maximum moment occurs obtained from numerical simulation is in good agreement with Kecman's stress distribution.
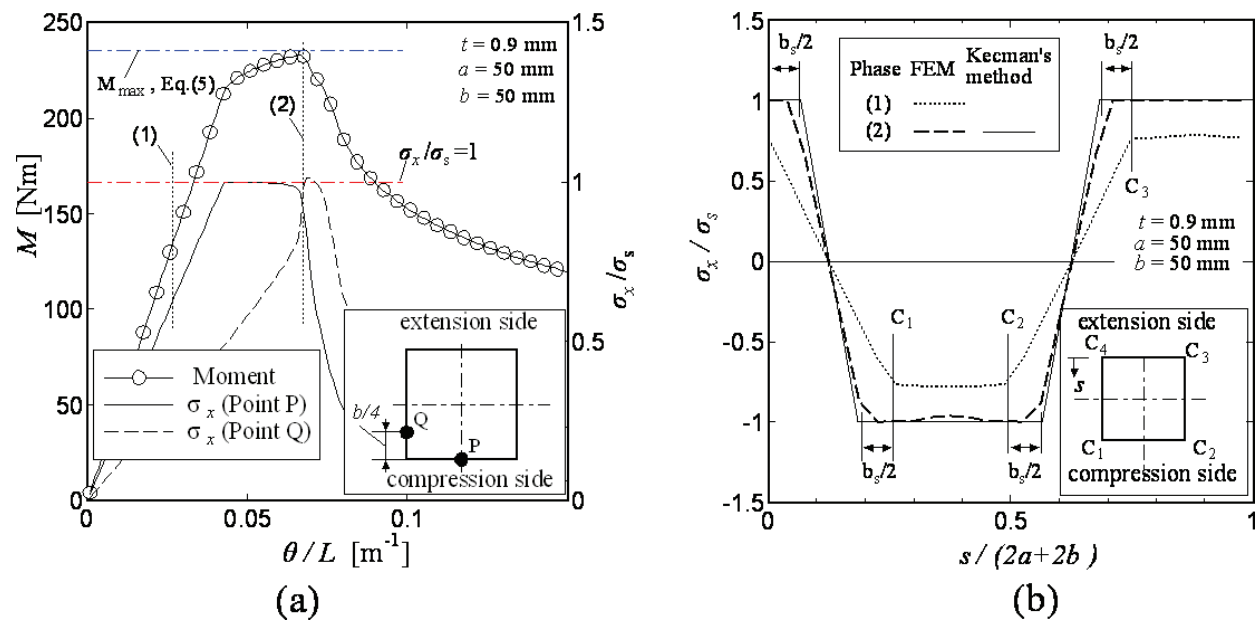

Figure 5. Moment M and axial stress σ_x on cross-section for a square tube with $t = 0.9$ mm, $a = b = 50$ mm are subjected to pure bending: (a) changes in moment M and axial stress σ_x at points P and Q on cross-section and (b) axial stress distribution on cross-section at phases (1) and (2) corresponding to $\theta/L = 0.025$ m⁻¹ and $\theta/L = 0.065$ m⁻¹, respectively, as denoted in (a).

The above investigation confirms that for such tubes with b/a = 1 and $\sigma_{buc\text{-}a} > \sigma_s$, the collapse is not due to buckling at the compression flange, but rather plastic yielding at the flange, and the maximum moment can be evaluated by Eq. (5) for Case 2.

3. To point out a case in which the estimation method is not applicable by using the results of numerical simulations

In order to investigate the accuracy of the Kecman's method for predicting the maximum moment M_{max} of tubes under bending, **Figure 6** shows the maximum bending moment of FEM numerical simulations for tubes with aspect ratios b/a = 1, 2, and 3. Eqs. (4), (5) and (6) are also shown as a comparison. As shown in the figure, the prediction of the Kecman's method is well in agreement with the results of FEM numerical simulations when the relative thickness t/a is not very small and the aspect ratio of web to flange b/a is not large, for example, when the tube relative thickness is about t/a > 0.008 for b/a = 1 and is about t/a > 0.016 for b/a = 2. However, for large aspect ratios, there is a large discrepancy between the values of maximum moment obtained from the Kecman's method and the FEM numerical results. This means that tubes with cross-section of a large aspect to which the Kecman's method does not apply are found
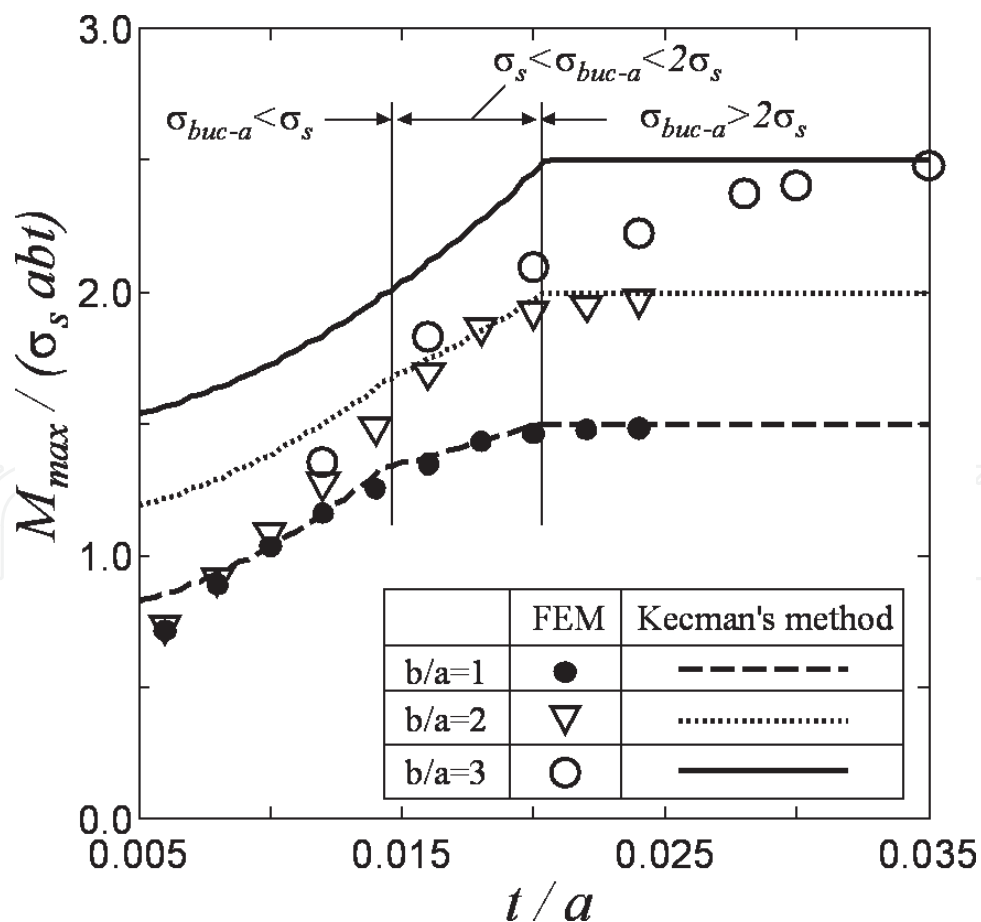

Figure 6. Comparison of the Kecman's method and the FEM numerical results.

to exist. Therefore, it is necessary to investigate the bending collapse mechanism of rectangular tubes in order to give an effective method for predicting the maximum moment of tubes.

4. To understand a factor of the discrepancy by using the results of numerical simulations

We investigate three tubes to which the Kecman's method is not applicable.

Figure 7 shows the bending moment M and the axial stress σ_x on cross-section for a rectangular tube with $t = 0.4$ mm, $a = 50$ mm, $b = 100$ mm ($\sigma_{buc\text{-}a} = 0.30\sigma_s$). As shown in **Figure 7(a)**, the maximum moment is less than the value obtained from Eq. (4) for Case 1. The maximum value of σ_x at point P is in good agreement with the elastic buckling stress $\sigma_{buc\text{-}a}$ given by Eq. (2), and the maximum value occurs before the maximum moment. Meanwhile, the axial compression stress σ_x at point Q at the quarter-web width decreases also before the moment becomes the maximum moment. Moreover, as shown in **Figure 7(b)**, the axial stress in the compression flange is concentrated at the edges when the maximum moment occurs, and the axial stress on the compression web does not change linearly. This suggests that compression buckling also arises at the web. Therefore, the axial stresses on the web at the maximum moment are less than that obtained by the Kecman's method, as indicated by the arrows in **Figure 7(b).**

The above investigation reveals that, in cases when b/a are large and $\sigma_{buc\text{-}a} < \sigma_s$, the collapse is not only due to buckling at the compression flange but also due to buckling at the compression web. Therefore, the maximum moment cannot be predicted by the Kecman's method. Based on **Figure 7(b)**, the cross-sectional stress distribution under the maximum moment corresponding to this collapse mode can be schematically represented by **Figure 8(a)** and called Case 4 in this chapter.

Figure 9 shows the bending moment M and the axial stress σ_x on cross-section for a rectangular tube with $t = 0.5$ mm, $a = 20$ mm, and $b = 100$ mm ($\sigma_{buc\text{-}a} = 2.83\sigma_s$). As shown in **Figure 9(a)**, the maximum moment is less than that obtained from Eq. (6) for Case 3. The axial compression stress σ_x at point P in the middle of the compression flange increases until the moment becomes the maximum moment, and the value σ_x/σ_s becomes approximately 1. However, the axial compression stress σ_x at point Q at the quarter-web width decreases before the moment becomes the maximum moment. Also, as shown in **Figure 9(b)**, the axial stress distribution in the compression flange is almost constant, and the absolute value of σ_x/σ_s is approximately 1 when the maximum moment occurs. However, as compared with Case 3 shown in **Figure 2(c)**, it is found that although the buckling stress of the flange $\sigma_{buc\text{-}a}$ obtained from Eq. (2) is higher than twice the yielding stress, $\sigma_{buc\text{-}a} = 2.83\sigma_s > 2\sigma_s$, a plastic yielding region is not found in the web. Moreover, the axial stress in the web does not change linearly and decreases greatly in the compression portion of the web. This suggests that compression buckling arises at the web. Therefore, the axial stress distribution at the maximum moment differs greatly from that obtained by the Kecman's method, as indicated by the arrows in **Figure 9(b)**, because in the Kecman's method, the buckling of web is not taken into account.
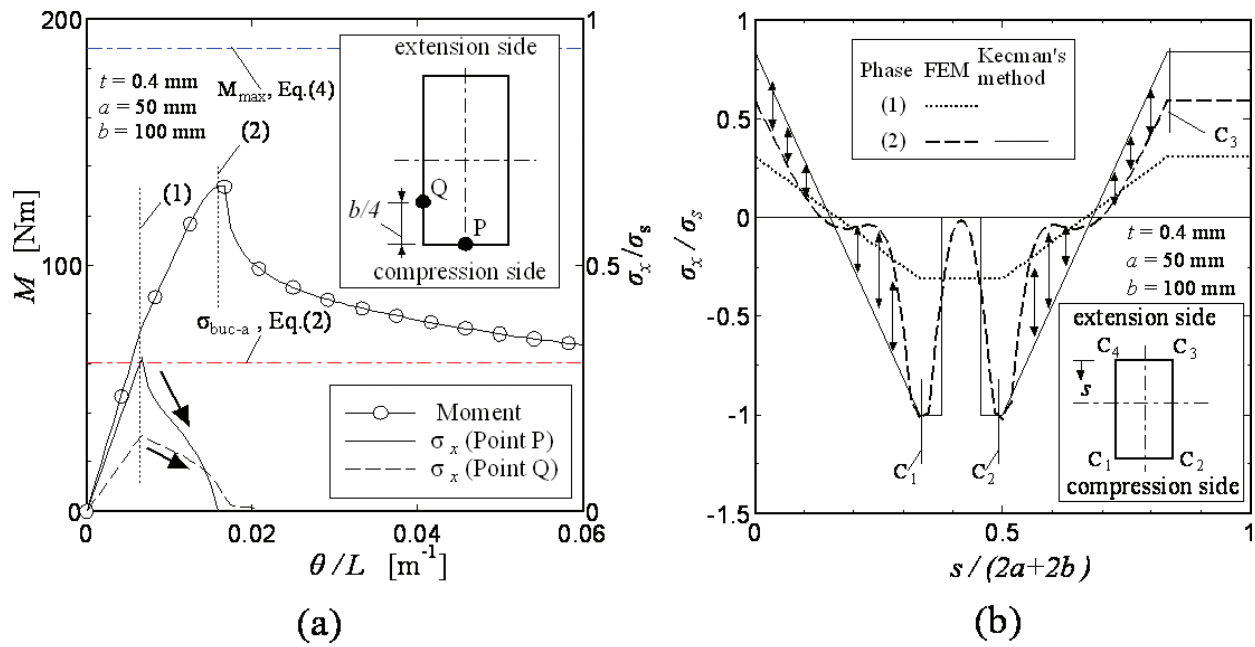
Figure 7. Moment M and axial stress σ_x on cross-section for a rectangular tube with $t = 0.4$ mm, $a = 50$ mm, $b = 100$ mm are subjected to pure bending: (a) changes in moment M and axial stress σ_x at points P and Q on cross-section and (b) axial stress distribution on cross-section at phases (1) and (2) corresponding to $\theta/L = 0.007$ m^{-1} and $\theta/L = 0.016$ m^{-1}, respectively, as denoted in (a).
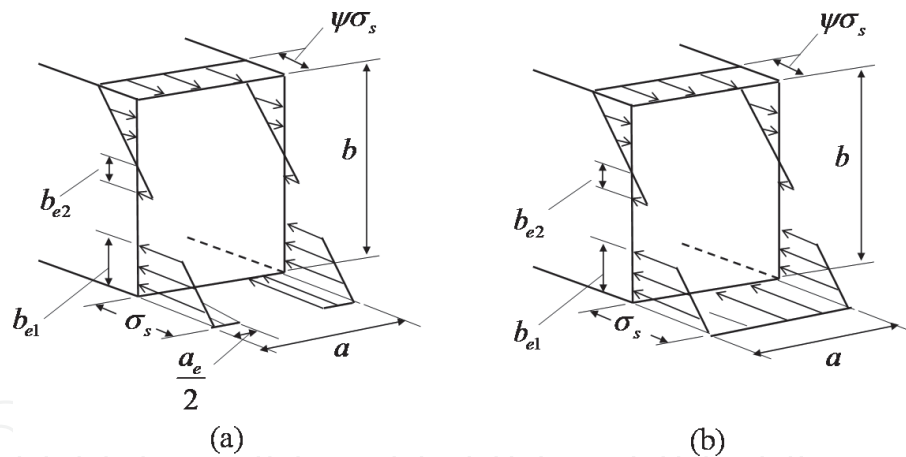

Figure 8. Schematic representation of axial stress distribution with considering the buckling at web when the maximum moment occurs: (a) case 4: $\sigma_{buc-a} < \sigma_s$ and (b) case 5: $\sigma_{buc-a} > \sigma_s$.

The above investigation reveals that, in such tubes with large aspect ratio b/a, even though $\sigma_{buc-a} > \sigma_s$, collapse is not due to plastic yielding at the flange, but rather buckling at the compression web in a state of plastic yielding at the compression flange. Therefore, the maximum moment cannot be predicted by the Kecman's method. Based on **Figure 9(b)**, the cross-sectional stress distribution under the maximum moment corresponding to this collapse mode can be schematically represented by **Figure 8(b)** and called Case 5 in this chapter.
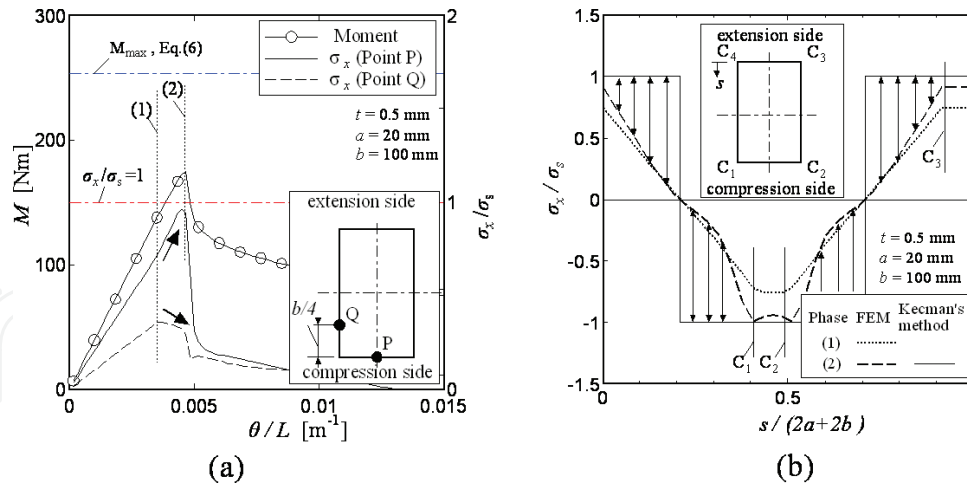
Figure 9. Moment M and axial stress σ_x on cross-section for a rectangular tube with $t = 0.5$ mm, $a = 20$ mm, $b = 100$ mm are subjected to pure bending: (a) changes in moment M and axial stress σ_x at points P and Q on cross-section and (b) axial stress distribution on cross-section at phases (1) and (2) corresponding to $\theta/L = 0.036$ m^{-1} and $\theta/L = 0.048$ m^{-1}, respectively, as denoted in (a).

Figure 10 shows the bending moment M and the axial stress σ_x on cross-section for a rectangular tube with $t = 1.2$ mm, $a = 50$ mm, $b = 150$ mm ($\sigma_{buc-a} = 2.8\sigma_s$). As shown in **Figure 10(a)**, the maximum moment is less than that obtained from Eq. (6) for Case 3. The axial compression stress σ_x at point P in the middle of the compression flange increases up to the yielding stress σ_s before the maximum moment was reached and sets the value σ_x/σ_s equal approximately to 1 until the moment becomes the maximum moment. However, the axial compression stress σ_x at point Q at the quarter-web width increases until the moment becomes the maximum
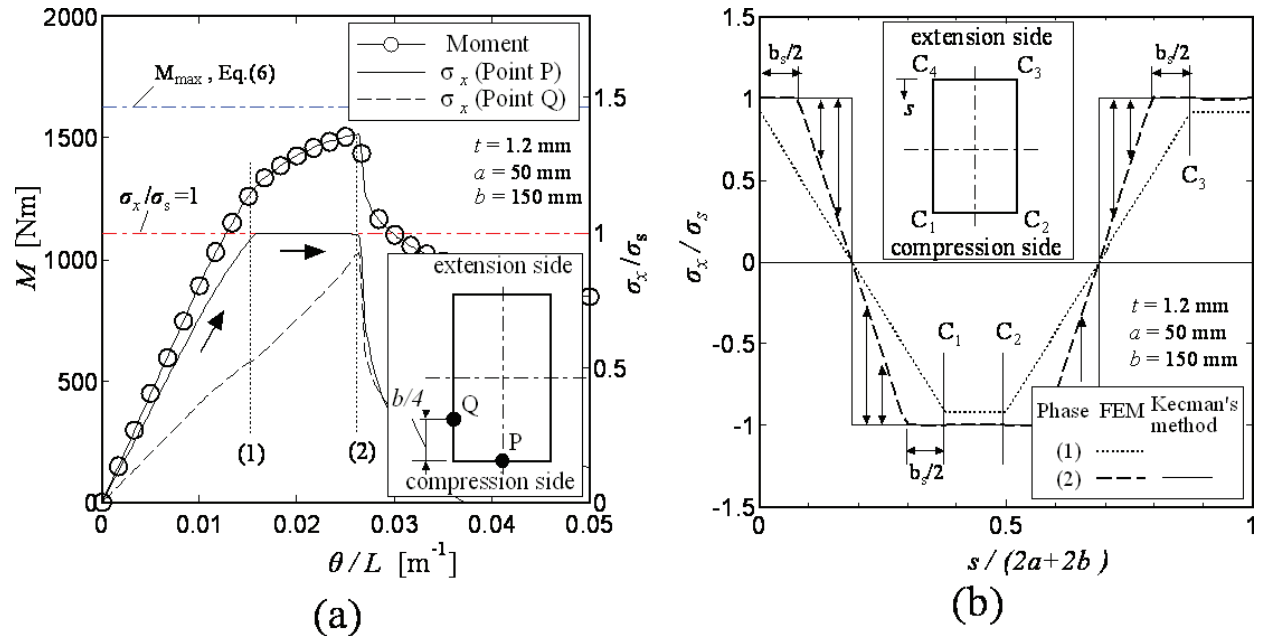

Figure 10. Moment M and axial stress σ_x on cross-section for a rectangular tube with $t = 1.2$ mm, $a = 50$ mm, $b = 150$ mm are subjected to pure bending: (a) changes in moment M and axial stress σ_x at points P and Q on cross-section and (b) axial stress distribution on cross-section at phases (1) and (2) corresponding to $\theta/L = 0.015$ m^{-1} and $\theta/L = 0.026$ m^{-1}, respectively, as denoted in (a).

moment. Also, it is seen from **Figure 10(b)** that the axial stress distribution in the compression flange is almost constant, and the absolute value of σ_x/σ_s is approximately 1 when the maximum moment occurs. Moreover, it is also found from a comparison with **Figure 9(b)** that in the web, no buckling occurs, but plastic yielding regions can be observed. However, the plastic yielding is not generated to the entire web, although the buckling stress of the flange $\sigma_{buc\text{-}a}$ obtained from Eq. (2) is higher than twice the yielding stress, $\sigma_{buc\text{-}a} = 2.8\sigma_s > 2\sigma_s$. Thus, the stress distribution is different from the cross-sectional fully plastic yielding, as indicated by the arrows in the figure. This suggests that even if a compression buckling does not arise at the web, the web slenderness also affects the cross-sectional fully plastic yielding of the tube under bending. That is, the conditions of generating the cross-sectional fully plastic yielding are dependent not only on the flange slenderness but also on the web slenderness. In the Kecman's method, the conditions for the cross-sectional fully plastic yielding are determined by only the ratio of $\sigma_{buc\text{-}a}$ to σ_s.

The above investigation reveals that in such tubes with large aspect ratio b/a, even though $\sigma_{buc\text{-}a} > 2\sigma_s$, the cross-sectional stress distribution under the maximum moment corresponding to this collapse mode may differ from that of the cross-sectional fully plastic yielding. Therefore, the maximum moment for such tubes cannot be predicted by the Kecman's method.

5. To propose a new estimation method by considering the factor and using mathematical approach

5.1. Effect of the web slenderness on the buckling at web

Bending stress occurs in the web of tube. The problem of web buckling is expressed in **Figure 11**. In **Figure 11(a)**, plate ABCD is defined by the width b and thickness t. As a boundary condition, displacement in the out-of-plane direction (displacement in the z direction) is fixed at both longitudinal edges (BC and DA). The bending and compression are applied through displacement control. For the ultimate loading after buckling, the distribution of compressive stress σ_x along the width direction is characterized by two effective widths, b_{e1} and b_{e2}, as shown in **Figure 11(b)**. In the figure, compressive stress is denoted by a positive value.

Many studies have been reported on the ultimate loading of a plate after buckling under bending and compression. For example, the effective widths b_{e1} and b_{e2} for a plate under stress gradient shown in **Figure 11** are given in AS/NZS 4600 standard [4] and NAS [5] as follows:

$$\begin{cases} b_{e1} = \dfrac{b_e}{3-\psi} \\[2mm] b_{e2} = \begin{cases} b_e/2 & when\ \psi \leq -0.236 \\ b_e - b_{e1} & when\ \psi > -0.236 \end{cases} \end{cases} \tag{10}$$

In addition, $b_{e1} + b_{e2}$ shall not exceed the compression portion of the web. Here, ψ is ratio of f_1^* and f_2^*. f_1^* and f_2^* are web stresses shown in **Figure 11(b)**.
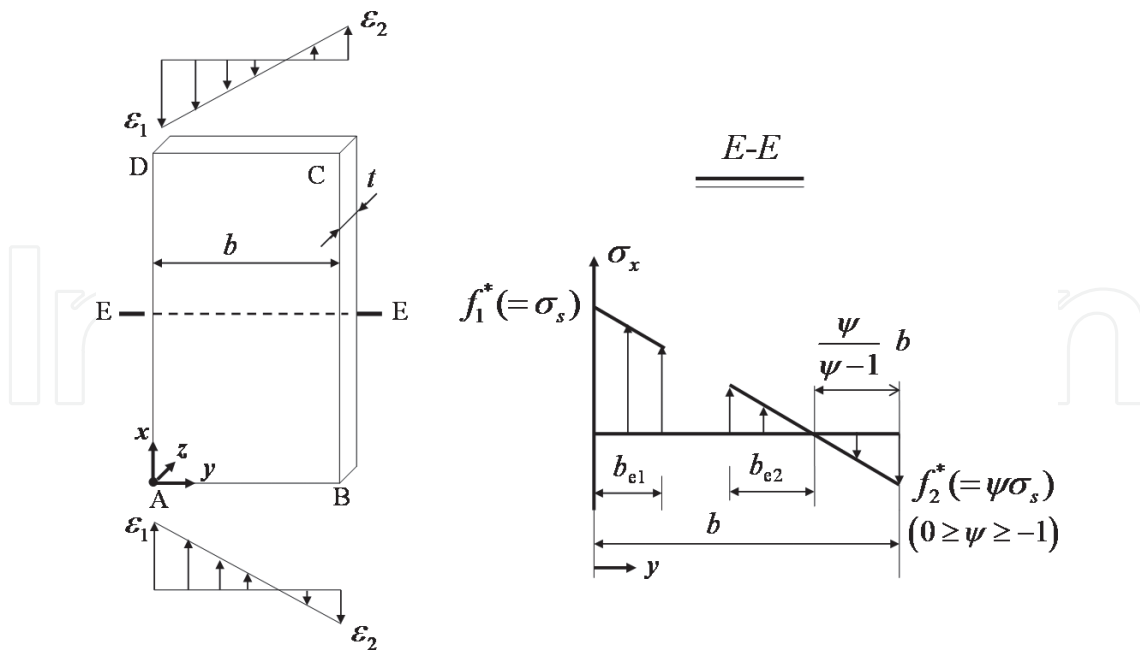
$$\psi = \dfrac{f_2^*}{f_1^*} \tag{11}$$

Figure 11. Plate subjected to compression and bending: (a) analyzed model and (b) axial compressive stress σ_x distribution on E–E cross-section in (a).

λ is defined by

$$\lambda = \sqrt{\frac{\sigma_s}{\sigma_{buc-b}}} \tag{12}$$

The elastic buckling stress of web σ_{buc-b} is calculated as follows:

$$\sigma_{buc-b} = \frac{k_b \pi^2 E}{12(1-v^2)}\left(\frac{t}{b}\right)^2 \tag{13}$$

where the buckling coefficient k_b is given by

$$k_b = 4 + 2(1-\psi)^3 + 2(1-\psi) \tag{14}$$

b_e is given by

$$b_e = \rho b \tag{15}$$

ϱ is called the reduction factor and is given by

$$\rho = \frac{1}{\lambda} \tag{16}$$

which is proposed by von Karman et al. [6]. The following formula for ϱ:

$$\rho = \frac{1}{\lambda}\left(1 - \frac{0.22}{\lambda}\right) \tag{17}$$

is also proposed by Winter [7] and is well used for design specifications. The reason of Eq. (15) modified to Eq. (17) in actual design is mainly due to the fact that the maximum load capacity

of a buckling plate is reduced greatly by imperfections when the buckling stress is close to the yield stress [8]. Therefore, Eq. (16) is desirable for the present model because the influence of imperfections is not taken into consideration here. Moreover, in order to consider continuity of the load capability of a web with $\lambda = 1$, for which elastic buckling does not occur because $\sigma_{\text{buc-b}} = \sigma_s$, we apply Eq. (16) to the present study.

Eq. (10) is applied to the webs investigated in **Figures 7(b)** and **9(b)** to determine the corresponding effective width; the stress distributions on the web based on the obtained effective width using Eq. (10) are shown in **Figures 12(a)** and **13(a)**. In **Figure 12(a)**, the stress distribution obtained using Eq. (10) is qualitatively corresponding with the redistribution of the compression stress after buckling obtained from the FEM numerical simulation. However, in **Figure 13(a)**, even though there is a fall of the compression stress in the compression portion of the web after buckling as shown by the FEM simulation, the stress distribution obtained from Eq. (10) looks like a straight line because the effective widths b_{e1} and b_{e2} determined by Eq. (10) satisfy the following equation:

$$b_{e1} + b_{e2} = \frac{b}{1 - \psi} \tag{18}$$

which means $b_{e1} + b_{e2}$ is equal to the compression portion of the web.

In fact, when the effective width is determined using Eq. (10), there are many instances in which Eq. (18) is satisfied. **Figure 14** shows various possible values of buckling stress of web, for which Eq. (18) is satisfied, for various assumed stress ratios ψ by solid line, as evaluated in Eq. (10) with ϱ defined in Eq. (16). In **Figure 14**, the dashed line shows the corresponding result if ρ was calculated using Eq. (17); it is also seen from the dashed line that even if Eq. (17) is used for ρ the instances in which Eq. (18) is satisfied still exist. For these instances, the redistribution of the compression stress after buckling cannot be expressed by the effective width obtained from Eq. (10); this means that there is a possibility of giving a too large load
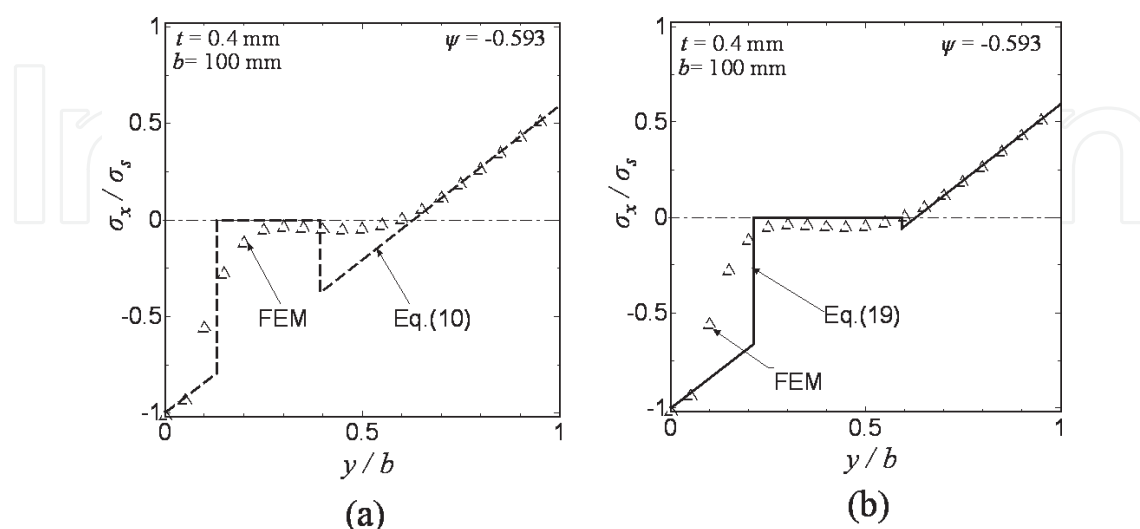

Figure 12. Stress distribution of web when the ultimate load is reached for the tube used in **Figure 7(b)**: (a) comparison with Eq. (10) and (b) comparison with Eq. (19).

capability of web from Eq. (10). Therefore, here as a comparison, we also use another solution given by Rusch and Lindner [9] which is given for the same plate shown in **Figure 11(a)** but with one of the two longitudinal edges BC being free. Although the free boundary condition at the longitudinal edge BC is different from the actual situation of web constituting the tube, the effect is assumed to be small because BC is under tension stress.
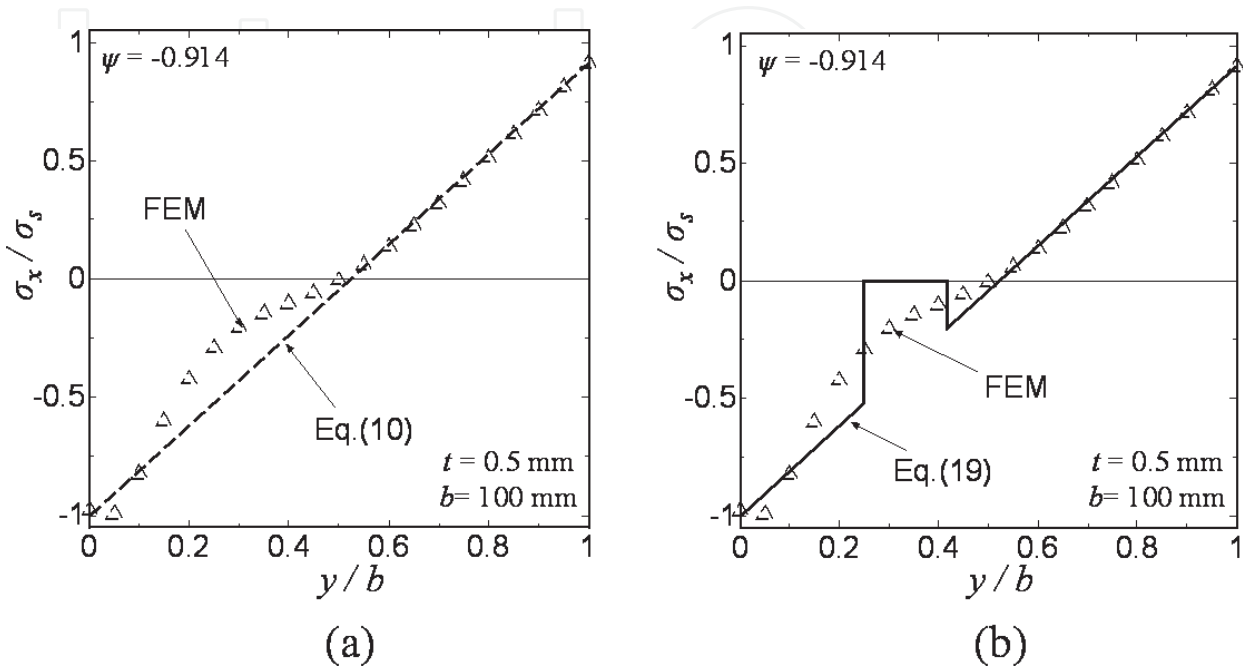

Figure 13. Stress distribution of web when the ultimate load is reached for the tube used in **Figure 9(b)**: (a) comparison with Eq. (10) and (b) comparison with Eq. (19).
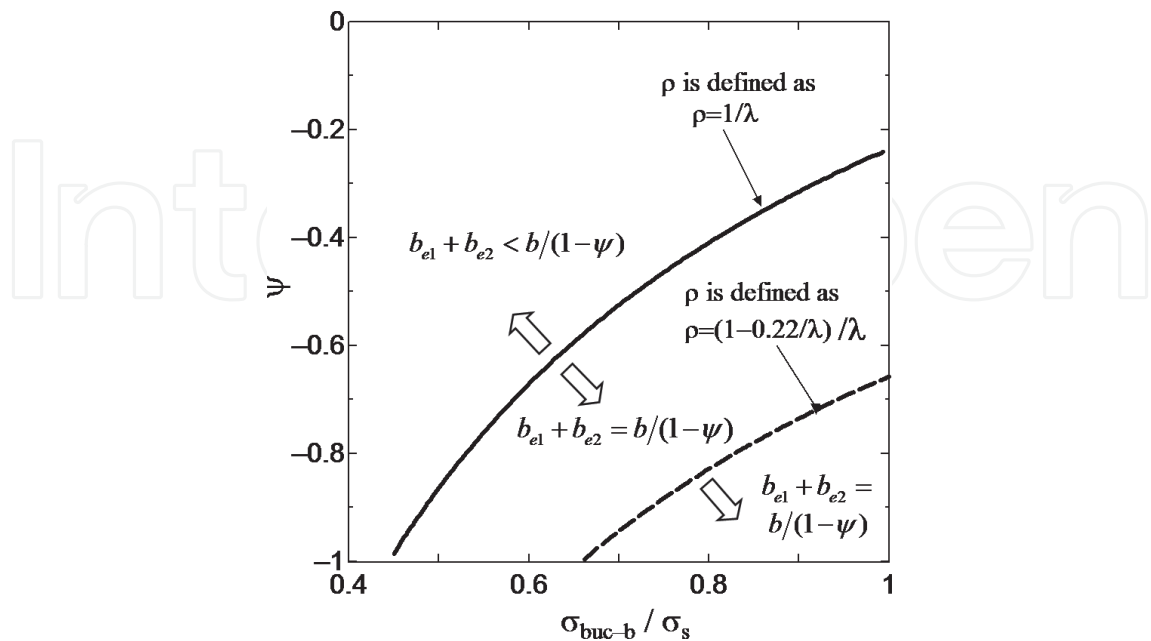

Figure 14. Various possible buckling stress $\sigma_{\text{buc-b}}$ and stress ratio ψ with Eq. (18) satisfied.

In Ref. [9], the effective widths b_{e1} and b_{e2} are given by

$$\begin{cases} b_{e1} = b_e - b_{e2} \\ \dfrac{b_{e2}}{b} = \dfrac{0.226}{\lambda^2} \end{cases} \qquad (19)$$

where

$$\frac{b_e}{b} = \frac{\rho}{1 - \psi} \qquad (20)$$

Here, λ and ρ are calculated by Eqs. (12) and (16), respectively, the buckling stress σ_{buc-b} is determined by Eq. (13) with k_b determined as follows:

$$k_b = 1.7 - 5\psi + 17.1\,\psi^2 \qquad (21)$$

Figures 12(b) and **13(b)** show the comparisons of stress distributions on the web obtained from FEM and Eq. (19) for the tubes used in **Figures 7(b)** and **9(b)**, from which it is seen that the redistribution of stress after web buckling can be approximately expressed using Eq. (19). Comparing (a) and (b) in **Figure 12**, it is seen that for the stress distribution on the web in the tube used in **Figure 7(b)**, Eq. (19) is inferior in accuracy to Eq. (10). However, as shown in **Figure 13**, which shows the stress distributions on the web for the tube used in **Figure 9(b)**, although the fall of the compression stress in the compression portion of the web after buckling is not expressed by the solution obtained from Eq. (10), it is expressed by the solution from Eq. (19). In fact, it is seen from Eq. (20) that for the stress distribution on the web as obtained from Eq. (18), the length of $b_{e1} + b_{e2}$ is always smaller than the compression portion of the web.

5.2. Effect of the web slenderness on the cross-sectional fully plastic yielding

For tubes with large aspect ratio of web to flange, as an effect of web slenderness on the tube collapse, we considered the possible buckling of web and thus investigated the existence of Cases 4 and 5, as shown above. Hereafter, we consider the other effect of web slenderness on the cross-sectional fully plastic yielding.

As shown in **Figure 6**, for tubes with $b/a = 3$, there is a large discrepancy between Kecman's prediction and the FEM simulation. When the tubes are very thin (e.g., when $t/a < 0.02$ for $b/a = 3$) it is thought that the error generating is brought about because the web buckling was not taken into consideration in the Kecman's method. However, for the relatively thick tubes, the cause which produces the error is clearly different because buckling does not occur in such tubes. For example, for the tube with $b/a = 3$ and $t/a = 0.024$ shown in **Figure 10(b)**, even though the buckling stress of flange σ_{buc-a} calculated by Eq. (2) is $\sigma_{buc-a}/\sigma_s = 2.8 > 2$, the maximum moment M_{max} as evaluated by FEM numerical simulation is $M_{max}/M_{pl} \cong 0.9$, which is not in agreement with Eq. (6) for the case of $\sigma_{buc-a}/\sigma_s = 2$ in the Kecman's method. Here, buckling does not occur in the web either because $\sigma_{buc-b}/\sigma_s = 1.4 > 1$. Also, it is seen from **Figure 10(b)** that the stress distribution on the cross-section is different from that shown in **Figure 2(c)** for Case 3 corresponding to the cross-sectional fully plastic yielding. This fact means that the condition for reaching the cross-sectional fully plastic yielding is also related to the web slenderness.

In order to consider the effect of the web slenderness on the tube collapse, the condition of $\sigma_{buc-a} > 2\sigma_s$ for Case 3 or for $M_{max} = M_{pl}$ in the Kecman's method is replaced in the present study by the following condition:

$$\begin{cases} \sigma_{buc-a} \geq 2\sigma_s \\ \sigma_{buc-b} \geq 2\sigma_s \end{cases} \tag{22}$$

Here, σ_{buc-b} is determined assumed $\psi = -1$. When Eq. (22) is not satisfied, that is, when

$$\begin{cases} \sigma_s < \sigma_{buc-a} < 2\sigma_s \\ \sigma_{buc-b} \geq 2\sigma_s \end{cases} \tag{23}$$

or

$$\begin{cases} \sigma_{buc-a} \geq 2\sigma_s \\ \sigma_s < \sigma_{buc-b} < 2\sigma_s \end{cases} \tag{24}$$

or

$$\begin{cases} \sigma_s < \sigma_{buc-a} < 2\sigma_s \\ \sigma_s < \sigma_{buc-b} < 2\sigma_s \end{cases} \tag{25}$$

the stress on cross-section is expressed by Case 2 shown in **Figure 2(b)**. This fact can be confirmed from **Figure 10(b)** for which Eq. (24) is satisfied.

It is seen from the cross-sectional stress distribution shown in **Figure 10(b)** that the maximum moment in this case is dependent on the plastic yielding region in the web. Denoting the length of this plastic yielding region by b_s (see **Figure 2(b)**), the maximum moment can be evaluated through the value of b_s as follows:

for Case 2,

$$M_{max} = \sigma_s t \left[\frac{1}{6}(2 b^2 + 2 bb_s - b_s^2) + ab \right] \tag{26}$$

Substituting Eqs. (8), (9), and (26) into Eq. (5), b_s is obtained as

$$\frac{b_s}{b} = \begin{cases} 1 - \sqrt{2 - \left(\frac{t}{t_{ea}}\right)^2} & \left(for \ t_{ea} < t < \sqrt{2} \ t_{ea}\right) \\ 1 & \left(for \ t \geq \sqrt{2} \ t_{ea}\right) \end{cases} \tag{27}$$

where t_{ea} is the flange thickness for which the elastic buckling stress σ_{buc-a} obtained from Eq. (2) is equal to the yielding stress σ_s and is given by

$$t_{ea} = a \sqrt{\frac{12(1 - \nu^2)}{k_a \pi^2}} \sqrt{\frac{\sigma_s}{E}} \tag{28}$$

Eq. (26) means that the b_s is determined by the flange slenderness only when Eq. (23) is satisfied. Therefore, when Eq. (24) is satisfied, we also suppose that the b_s can be determined by the web slenderness only as follows:

$$\frac{b_s}{b} = \begin{cases} 1 - \sqrt{2 - \left(\frac{t}{t_{eb}}\right)^2} & \left(for\ t_{eb} < t < \sqrt{2}\ t_{eb}\right) \\ 1 & \left(for\ t \geq \sqrt{2}\ t_{eb}\right) \end{cases} \tag{29}$$

where t_{eb} is the web thickness for which the elastic buckling stress $\sigma_{buc\text{-}b}$ is equal to the yielding stress σ_s and is given by

$$t_{eb} = b \sqrt{\frac{12(1 - \nu^2)}{k_a \pi^2}} \sqrt{\frac{\sigma_s}{E}} \tag{30}$$

Furthermore, we assume that this technique can also be used to evaluate the maximum moment in the case when Eq. (25) is satisfied. That is, M_{max} is determined from the smaller one from both values of b_s given in Eq. (27) and in Eq. (29). Validity of this assumption can be understood from **Figure 16(b)** shown later, in which for the tube with $t/a = 0.016$, Eq. (25) is satisfied: $\sigma_{buc\text{-}a} = 1.23\sigma_s$ and $\sigma_{buc\text{-}b} = 1.39\sigma_s$. Therefore, when using Eq. (26) to determine M_{max} for Case 2, the value of b_s is calculated using Eq. (27) if

$$t_{ea} > t_{eb} \tag{31}$$

and is calculated using Eq. (29) if

$$t_{ea} < t_{eb} \tag{32}$$

Using t_{ea} and t_{eb}, the condition of Eq. (22) can be rewritten as.

$$t \geq \sqrt{2}\ t_{ea}\ and\ t \geq \sqrt{2}\ t_{eb} \tag{33}$$

5.3. Estimation of collapse load for thin-walled rectangular tubes under bending

Figure 15 shows a flow chart of a new method proposed in the present study for predicting the maximum moment of tubes under pure bending. This method includes both the possible buckling at web and the effect of web slenderness on the cross-sectional fully plastic yielding. In the flow chart, $\sigma_{buc\text{-}b,1}$ and $\sigma_{buc\text{-}b,2}$ are the buckling stress of web assuming the stress ratio ψ to be

$$\psi = -\frac{b - y_1}{y_1} = -\frac{a_e + b}{a + b} \tag{34}$$

and $\psi = -1$, respectively. Moreover, it is notable that in calculating the maximum bending moment for Cases 4 and 5 the stress ratio ψ is also unknown, which shall be determined from the conditions of pure bending through trial and error. Using the determined value of ψ, the maximum moment for Cases 4 and 5 is calculated as follows:

for Case 4:

$$\frac{M_{max}}{\sigma_s t} = \psi \left[b^2 + d_1^2 - d_2^2\right] + \frac{2(1 - \psi)}{3b}\left[b^3 + d_1^3 - d_2^3\right] + a_e b \tag{35}$$
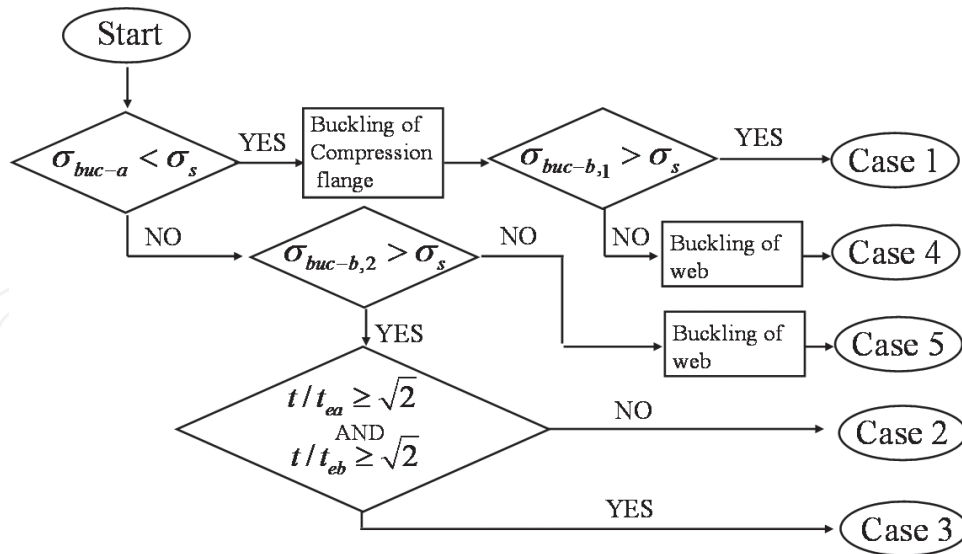
Figure 15. Flow chart of a new method proposed in the present study for predicting the maximum moment of tubes under pure bending.

for Case 5:

$$\frac{M_{max}}{\sigma_s t} = \psi\left[b^2 + d_1^2 - d_2^2\right] + \frac{2(1-\psi)}{3b}\left[b^3 + d_1^3 - d_2^3\right] + ab \tag{36}$$

In Eqs. (35) and (36).

$$d_1 = b_{e2} + \frac{\psi}{\psi-1}b, d_2 = b - b_{e1} \tag{37}$$

6. To understand the validity of the new estimation method by comparing with the results of numerical simulations

In **Figure 16**, the maximum moment predicted by the present method is compared with that obtained from the FEM numerical simulation with $a/b = 1$, 2, and 3 for **Figures 16(a)**, **16(b)**, and **16(c)**, respectively. As a result of the prediction method proposed in this chapter, "method 1" uses Eq. (10) and "method 2" uses Eq. (19) for calculating the effective width.

The case number of the collapse corresponding to each thickness is also shown in the figures. In Case 2, there are two possible subcases: (1) $t_{ea} > t_{eb}$ as shown in **Figure 16(a)** and **(b)** and (2) $t_{ea} < t_{eb}$ as shown in **Figure 16(c)**; the maximum moment is determined by Eq. (27) for the former and by Eq. (29) for the latter. As shown in these figures, Eqs. (27) and (29) give good prediction to the corresponding subcase, respectively.

For Cases 4 and 5, although each result obtained from methods 1 and 2 is approximately in agreement with the FEM results of numerical simulations, it is found that there is a gap in the results between methods 1 and 2. When the buckling stress of the web $\sigma_{buc\text{-}b}$ is close to
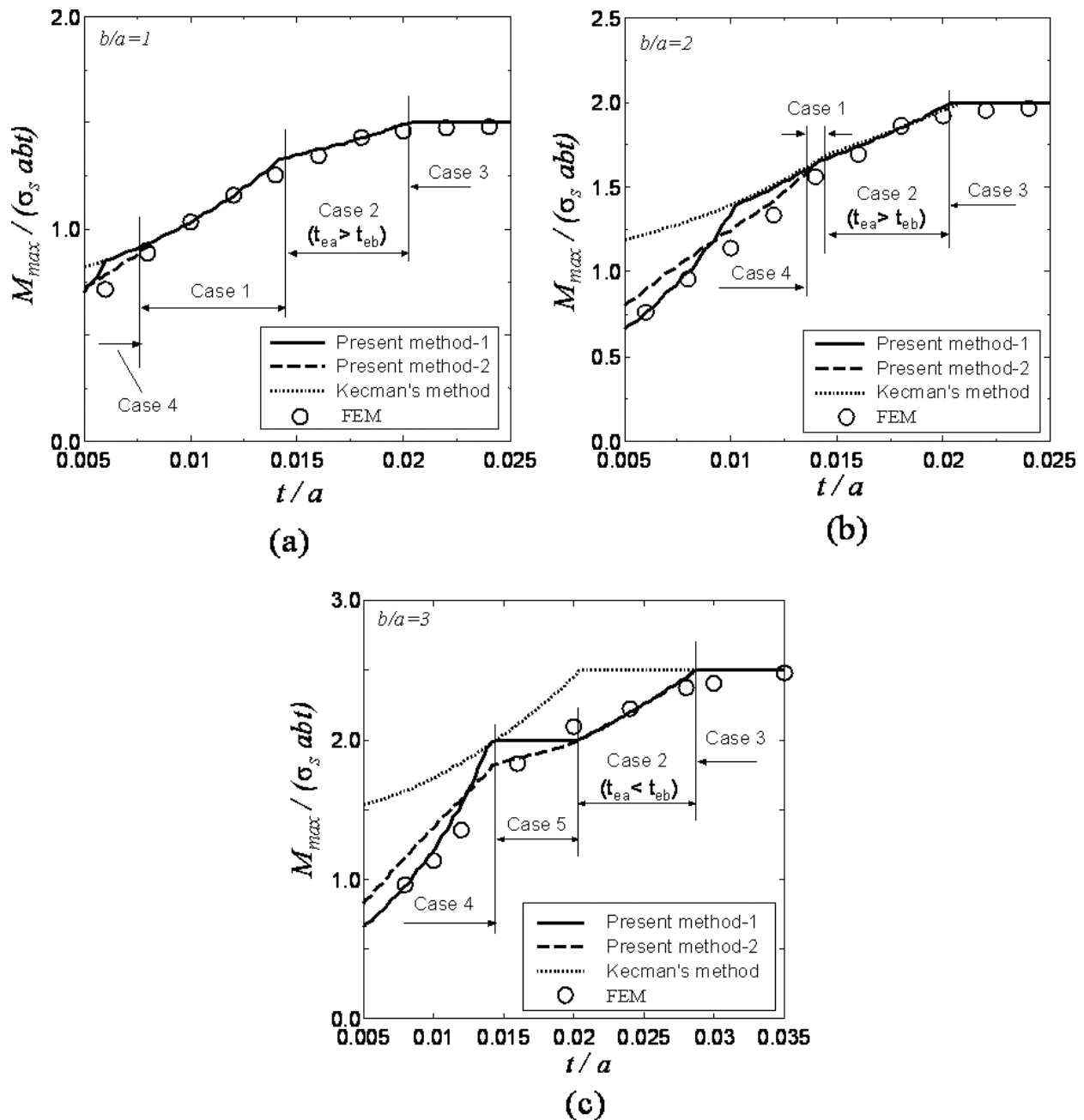
Figure 16. Prediction of the maximum bending moment M_{max} for rectangular tubes: (a) a/b = 1; (b) a/b = 2; and (c) a/b = 3.

the yielding stress σ_s, the method 1 gives a too large prediction as compared with the FEM results, reflecting the fact that $b_{e1} + b_{e2}$ given by Eq. (10) may be equal to the compression portion of the web as shown in **Figure 14**. However, for small t/a, when σ_{buc-b} is very much less than the yielding stress, method 1 is more accurate compared with method 2. Combining the advantages of these two methods, it is seen from **Figure 16(a)**, **(b)**, and **(c)** that the smaller one from both solutions obtained from method 1 and obtained from method 2 is in good agreement with the FEM results for all of Cases 4 and 5.

7. Conclusion

In this chapter, bending collapse of rectangular tubes was investigated using the FEM numerical simulation. The Kecman's method in which the post buckling strength of the flange and the effect of the flange slenderness on the cross-sectional fully plastic yielding are taken into account is effective when the aspect ratio of web to flange is not large. However, in order to predict accurately the maximum moments of rectangular tubes with large aspect ratio of web to flange, the slenderness of web has to be taken into account. Our new method in which the post buckling strength of the web under stress gradients and the effect of the web slenderness on the cross-sectional fully plastic yielding are taken into account are proposed, and the predicted maximum moment agrees with the results of FEM numerical simulations.

Author details

Kenichi Masuda[1]* and Dai-Heng Chen[2]

*Address all correspondence to: masuda@eng.u-toyama.ac.jp

1 Faculty of Engineering, University of Toyama, Toyama, Japan

2 National Center for International Research on Structural Health Management of Critical Components, Jiangsu University, Zhenjiang, China

References

[1] Kecman D. Bending collapse of rectangular and square section tubes. International Journal of Mechanical Sciences. 1983;**25**(9-10):623-636

[2] Chen HD, Masuda K. Estimation of collapse load for thin-walled rectangular tubes under bending. ASME Journal of Applied Mechanics. 2016;**83**:031012-1-031012-8. DOI: 10.1115/1.4032159

[3] Guarracino F. On the analysis of cylindrical tubes under flexure: Theoretical formulations, experimental data and finite element analyses. Thin-Walled Structures. 2003;**41**:127-147

[4] AS/NZS 4600, editor. Cold-formed steel structures. Australian/New Zealand standard: Standards Australia; 2005

[5] NAS, editor. AISI Standard. 2004 supplement to the North American specification for the design of cold-formed steel structural members 2001 edition. American Iron and Steel Institute; 2004

[6] Karman VT, Sechler EE, Donnell HL. Strength of thin plates in compression. The American Society of Mechanical Engineers. 1932;**54**:53-57

[7] Winter G. Strength of thin steel compression flanges. Transactions of the American Society of Civil Engineers. 1947;**112**:527-554

[8] Rhodes J. Buckling of thin plates and members-and early work on rectangular tubes. Thin-Walled Structures. 2002;**40**(2):87-108

[9] Rusch A, Lindner J. Application of level I interaction formulae to class 4 sections. Thin-Walled Structures. 2004;**42**(2):279-293